Experimental Validation of Stable Equilibria in Fuel Cells with Dead-Ended Anodes

Jixin Chen, Jason B. Siegel, Toyoaki Matsuura, Anna G. Stefanopoulou and Serhat Yesilyurt

Abstract— This paper investigates the nitrogen blanketing front during the dead-ended anode (DEA) operation of a PEM fuel cell. Surprisingly the dynamic evolution of nitrogen and water accumulation in the dead-ended anode (DEA) of a PEM fuel cell arrives to a steady-state suggesting the existence of equilibrium behavior. We use a multi-component model of the two-phase one-dimensional (along-the-channel) system behavior to analyze and exploit this phenomenon. Specifically, the model is first verified with experimental observations, and then utilized for showing the evolution towards equilibrium. The full order model is reduced to a second-order ordinary differential equation (ODE) with one state, which can be used to predict and amalyse the surprising but experimentally observed steady state DEA behavior.

I. INTRODUCTION

Dead-end anode (DEA) operation of a PEM fuel cell has been implemented by several groups [1], [2], [3] and applied to a commercial fuel cell module Nexa (1.2 KW stack of 42 cells) from Ballard Power Systems [4]. In DEA operation, hydrogen is fed into anode with regulated pressure at the inlet , whereas the cathode is operated with conventional flow-through conditions associated with a stoichiometry ratio (SR) greater than one. Since the Nafion membrane is not an ideal seperator, nitrogen and water can diffuse through the membrane from the cathode and accumulate in the anode due to the DEA. In a vertically oriented cell as shown in Fig. 1, the reaction driven convective transport of gas mixture towards the channel end, together with the diffusion, produces an along-the-channel hydrogen depletion and eventual starvation in the end-region. The spatial variation of the species in the anode results in uneven local current distribution, whereas the temporal depletion of hydrogen leads to decreasing cell voltage with time under galvanostatic operation. For example, in our 50 cm^2 DEA cell experiment, the voltage was dropping from 0.7 to 0.6 V in ~15 minutes with an current density of 0.4 A/cm^2 [5].

Purging of the anode is typically needed to release accumulated nitrogen and water and maintain a manageable voltage range. A purge, normally taking 20-900 ms, is implemented by a solenoid valve at the downsteam of the anode. Since the anode pressure is regulated at the upsteam of anode, the opening of solenoid valve leads to turbulent orifice flow which clears the nitrogen and water from the anode channels. The downstream purge valve and the upstream pressure regulator are the only hardware at the anode side
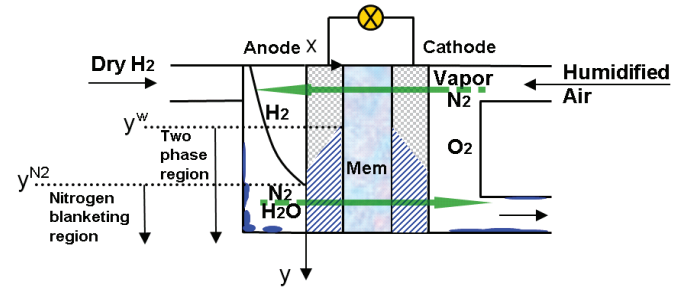
Fig. 1. Equilibrium scenario in DEA operation (not to scale). The net flux of nitrogen is from anode to cathode in the channel end-region, as opposed to other regions. Globally, zero net fluxes of nitrogen and water through the membrane are achieved at equilibrium.

for a DEA system. As a comparison, conventional flow-through anode (FTA) fuel cell system depends on a recirculation loop to maintain a high hydrogen utilization, which requires hydrogen grade plumbing and hardware such as an ejector/blower, water separator, and hydrogen humidifier. These components add weight, volume, and expense to the system. Note that in DEA system, the water crossing through the membrane humidifies the hydrogen fuel so that anode inlet humidification can be removed or reduced. In literature there are studies on improving the FTA system efficiency by optimizing the bleed rate and air supply [6], [7].

The DEA operation with periodic purge leads to varying cell voltage within the purge-period and requires additional power electronic to regulate the decreasing voltage. The additional complexity of the DEA voltage variability adds the overall system cost. Motivated by the experimental findings of [8], the possibility of operating the DEA cell without purging is analysed here. We address the conditions under which system equilibrium could be achieved with relatively stable voltage output under galvanostatic operation, and how to obtain a reasonable power under such equilibrium conditions. Voltage equilibrium was indeed observed in prior experimental studies [9], [10]. These findings motivate our further investigation by mechanism analysis and simulation using validated model.

As shown in Fig. 1, a stratified channel distribution with water and nitrogen in the end can be observed [3] for the DEA cell. In this case the local nitrogen partial pressure may easily exceed the cathode. Particularly in the channel end-region with nitrogen blanketing or hydrogen starvation, the nitrogen diffuses from the anode to the cathode due to the difference of its partial pressure as illustrated by the bottom arrow (positive x-direction). In the upper portion of the cell with substantial amount of hydrogen and thus small nitrogen partial pressure, the nitrogen crossover is from cathode to anode (negative x-direction). The nitrogen

blanketing front propagates until a global balance of nitrogen crossover has been achieved, meaning a zero net flux of nitrogen crossover. Since the nitrogen partial pressure in the anode is related to all other physical and eletrochemical parameters such as hydrogen partial pressure, local current and voltage, an equilibrium of nitrogen blanketing front drives the equilibrium of the whole DEA fuel cell system. There is a non-linear coupling of anode nitrogen partial pressure and membrane hydration which introduces complexity while analyzing such nitrogen equilibrium. The local electrochemical reaction rate depends on the hydrogen concentration, or nitrogen concentration due to regulated anode pressure, and determines the local water generation rate, which affects the membrane water content. The membrane pemeation coefficient for nitrogen, as a function of membrane water content and temperature, in turn influences the local nitrogen crossover rate and the establishment of nitrogen equilibrium.

In previous work [11], we have shown the effect of nitrogen accumulation in the anode on the voltage decay by modeling nitrogen crossover and convective transport in the anode with diffusion ignored. An one-dimensional, single-phase and transient model considering both convection and diffusion has been developed [12] to capture the spatiotemproral evolution of species and electrochemical reaction in a DEA cell. The model was further extended to include the cathode carbon corrosion caused by the anode fuel starvation and associated irreversible voltage degradation over time [13]. Recently, the model was improved to be 1+1D (along channel + through membrane) and two-phase so that the purge behavior can be predicted more accurately for an optimization study of purge scheduling [14]. After careful tuning, the present full-order-model can capture comprehensive mass transport and electrochemical processes in DEA operation with satisfactory accuracy when compared against data, which is a useful tool for predicting the equilibrium behavior [9], but several algebraic constraints, which requires numerical tools with substantial computational expense to solve the problem.

In this paper, therefore, we focus on reducing the state and order of the non-linear system. It is anticipated that a mathematical analysis can be performed on the reduced order system to determine the criteria for obtaining the DEA equilibrium, and the performance under equilibrium. There are similar works (simulation and analysis) focusing on the fuel cell equilibrium behavior from Benziger's group [15], [16], [17], [18]. However, those studies are based on a stirred-tank-reactor (STR) fuel cells which represents a simplified version of an operating cell that retains the essential physics. In their case both anode and cathode supplies are dry or slightly humidified to comply with the auto-catalytic concept of STR fuel cell and to create a scenario for water balance analysis. The effect of convective transport has been minimized by eliminating the need for channel flow. Although both STR and DEA cell feature self-himidification and spatial inhomogeneity, the equilibrium behavior in DEA cell represents a more complicated scenario where both diffusion and convection are considered. The convection leads to the stratified channel distribution of gas species in the vertically oriented cell. The diffusive transport in the channel is equally important by moderating the effect of nitrogen blanketing in the anode channel.

The remaining of this paper is organized as follows: our model has been detailed in prior works [13], [14] with an overview in this paper, and model validation against the flow-through polarization and DEA degradation test data will be presented. It will be shown that the tuned model predicts the voltage evolution towards equilibrium in DEA operation, achieving satisfactory agreement with the experimental data. The model is also used to simulate the nitrogen accumulation towards equilibrium in the anode. After presenting the equilibrium, we will perform a mathematical analysis on the criteria for achieving equilibrium. The analysis focuses on derivation of a single-state and reduced-order system to describe the nitrogen blanketing front. The solution to the algebraic equation of nitrogen blanketing front will then determines the existence of equilibrium in DEA operation.

II. Model Summary and Validation

The present model is 1+1D, two-phase and transient, which generally captures all transport phenomenon and reaction kinetics in the vertically oriented DEA cell with affordable computational expense. The model framework is reviewed briefly in Table I. The state n_i (i=[1,2,3]) denotes the molar fraction of nitrogen/vapor/oxygen, the hydrogen molar faction can be then determined since $\Sigma n_i = 1$. There are three liquid water related states in the anode, s, $s_{ctl,an}$ and x_{fr}. The first and second one describe the liquid volume fraction in the channel and catalyst layer; and the third one indicates the liquid water front in the GDL. The governing equation for s includes convection, diffusion, and source term, which comes from the vapor condensation and liquid transport from the GDL. Only when x_{fr} reaches the interface of GDL and channel can the liquid water enter the channel from the GDL. The state λ_{mb} indicates the membrane water content which is governed by water balance in the membrane. There is also a state m_C capturing the decreasing cathode carbon mass with time. Finally, cell voltage (E_{cell}) and interfacial potential at anode (ϕ_{AN}) are two variables constrained by two algebraic equations. All these states constitute a coupled multi-state second order non-linear system which requires numerical tool to solve.

The model parameters relevant to the species distribution in the anode have been tuned in prior works [12], [13]. These parameters include the nitrogen permeation scale factor, the oxygen crossover scale factor, and the concentration parameter for hydrogen reaction which affects the hydrogen consumption rate. They are kept unchanged whereas two other sets of parameters are further tuned. The first group is the cell polarization related parameters: the exchange current density of oxygen reaction (i_{0,O_2}) and the contact resistance (R_{GDL}). The second group is the carbon corrosion related parameters: the exchange current density of carbon corrosion (i_C) and the power factor for estimating the remaining carbon (q). The simulation results from tuned model together with

TABLE I

SUMMARY OF MODELING EQUATIONS

State/Variable	Governing Equation	Reference
n_i	$\frac{P_{an}}{RT}\frac{\partial(1-s)n_i}{\partial t} = -\frac{\partial}{\partial y}(J_i + n_i N_t) + r_i$	[12], [13]
s	$\rho_w \frac{\partial s}{\partial t} = \rho_w D_s \frac{\partial^2 s}{\partial y^2} - \rho_w \frac{RT}{P_{AN}}\frac{\partial[f(s)N_t(y)]}{\partial y} + M_w(r_{V,cond} + \frac{N_{l,an}(x=\delta_{GDL})}{d_{ch}})$	[14]
λ_{mb}	$\frac{\partial \lambda_{mb}}{\partial t} = \frac{EW}{\rho_{mb}\delta_{mb}}(N_{w,ca,mb} - N_{w,an,mb})$	[19]
x_{fr}	$\frac{\partial x_{fr,an}}{\partial t} = K_L N_{l,an}$	[19]
m_C	$\frac{\partial m_C(y,t)}{\partial t} = -\frac{M_C i_{C,CA}}{4F}$	[13]
$s_{ctl,an}$	$\lambda_{an} = (1 - s_{ctl,an})\lambda^* + s_{ctl,an}\lambda_{max}$	[19]
E_{cell}, ϕ_{AN}	$i_{AN} + i_{CA} = 0, i_{fc} = \frac{1}{L}\int_0^L i_{AN}dy$	[13]

the experimental data used for tuning are presented in Figs. 2 and 3.

The polarization performance obtained from flow-through operation is shown in Fig. 2. The DEA model is used to predict flow-through operation by assigning a constant to the flux at the anode outlet N_{out} [14] so that the desired anode SR, defined as the ratio of the total enthalpy of consumed hydrogen over the total fuel cell energy output, is achieved. The model prediction shows satisfactory agreement with experimental data. The model can predict the performance improvement due to increased cathode pressure and RH, although the difference is limited as cathode pressure increases from 2 to 4 and 10 psig. At elevated current densities, the model over-estimates the voltage probably because the influence of liquid water on the oxygen transport in the cathode channel is not modeled. In the conditions of 100% cathode supply RH, 2.5 cathode SR, and increased current, the presence of liquid water in the cathode is inevitable. When cathode RH has been reduced to 50%, the model prediction is closer to the experimental data at elevated current densities. The satisfactory agreement at small current densities is important since the model is used for studying DEA operation at low current densities.

Figure 3 illustrates the voltage evolution in three continuous DEA cycles in the beginning of life (BOL) and degradation over multiple cycles for two cases with different cathode supply RH. DEA cycle corresponds to the very repeatable voltage behavior between two consecutive purges. In Fig. 3, the agreement of BOL voltage evolution between two consecutive purges demonstrates the validity of reaction kinetics and gas transport related parameters. The cell degradation is observed in the voltage after purge, V_{ap}, decreasing in time shown in the fifth subplot. When cathode RH is 100% the voltage decreases due to the well-predicted carbon corrosion, whereas when cathode RH is 50% the model under-estimates the decay. The irreversible voltage loss here is all attributed to carbon corrosion and associated Pt loss, which is assumed to be related to the ratio of remaining carbon versus original carbon mass [13]. Membrane degradation in reality also contributes to the voltage degradation in a form of polymer chemical decomposition and associated increased resistance, which proceeds more rapidly when the cathode is drier (RH 50%) [20]. The membrane degradation is not considered in the present model and is most likely the reason for discrepancy between modeling and experimental data. Fortunately, catactrophic memebrane failure such pin-

hole was not observed in the DEA operation with small or medium current load [5] which normally leads to rapid voltage drop and shutdown of the cell under galvanostatic operation [21].
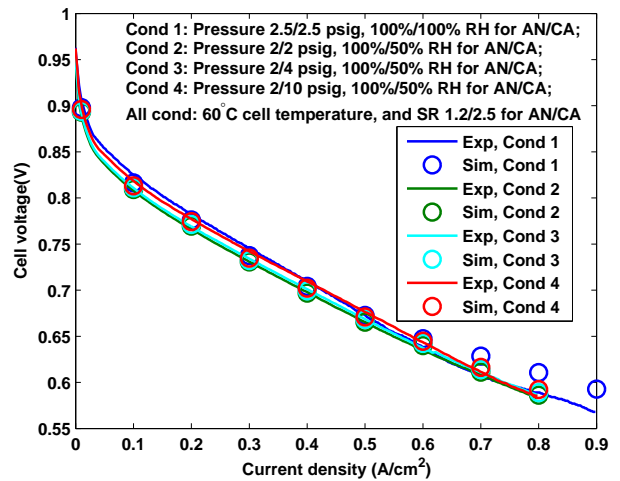

Fig. 2. The comparison of polarization performance between modeling and experimental data for 4 sets of operating conditions. The model can predict the polarization performance with acceptable accuracy.

The tuned model can predict a stable equilibrium in DEA operation when the purge is disabled, with satisfactory agreement as compared to the experimental data. Figure 4 shows two cases that achieved stable equilibrium in the experiment after ~100 minutes of DEA operation, as well as the simulation results with the same operating conditions. The experimental findings indicate that high cathode RH should be avoided to obtain a stable equilibrium since liquid accumulation causes localized shutdown. For the same reason, the cathode pressure was reduced to achieve the stable equilibrium (2.4 versus 4.0 psig in the anode), since smaller partial pressure of vapor is favorable for water diffusion from anode to cathode. The stable equilibrium was achieved with cathode supply RH of 60%. Generally, the humidified cathode supply introduces additional complexity and randomness in DEA equilibrium. For example, the erratic voltage behavior after reaching equilibrium can be attributed to liquid water condensation in the channel, which forms droplets that randomly block the channel before falling to the bottom of the channel. Humidified cathode supply, on the other hand, may improve the DEA cell performance by
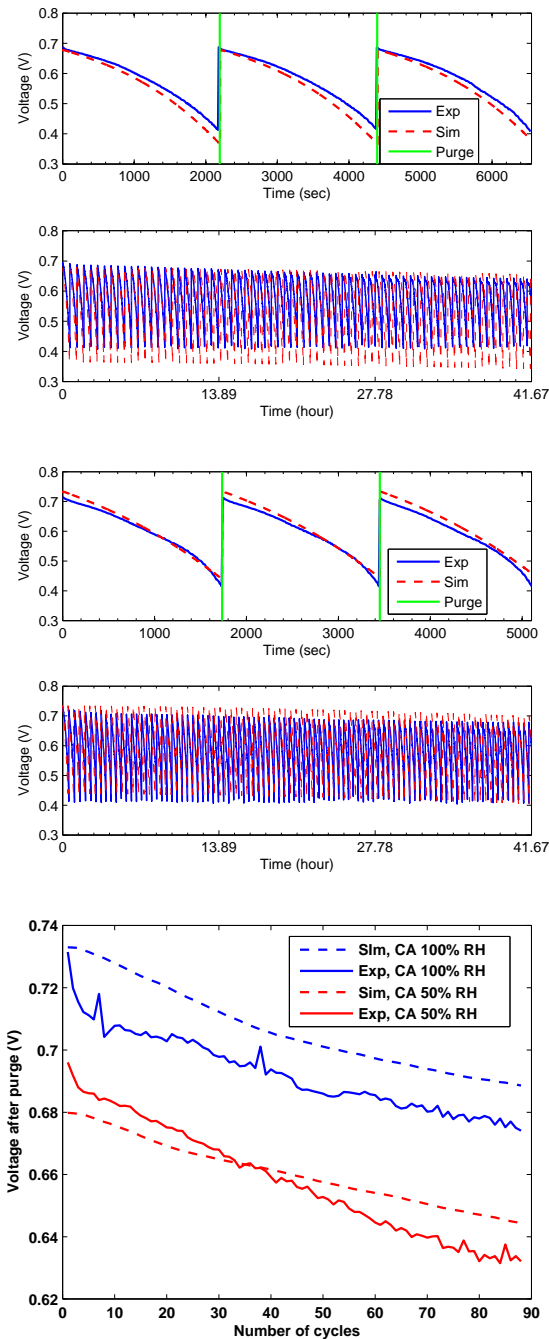
Fig. 3. The comparison of cell voltage evolution within three continuous cycles in the beginning of life and degradation over multiple cycles from both modeling and experimental data. The operating conditions are: cell temperature 60 °C and cathode supply 50% RH for the first two subplots; cell temperature 60 °C and cathode supply 100% RH for the third and fourth subplots. The cathode SR is 2.5 and both anode and cathode pressures are 3.8 psig; the current density is 0.4 A/cm^2. For a better illustration, the voltage after purge, V$_{ap}$, of each cycle is plotted against cycle number to show the degradation effect in the fifth subplot.

reducing the membrane ionic resistance particularly in the inlet region, only if the water from reaction is not sufficient to maintain necessary membrane hydration. Therefore, cathode humidification is usually not critical for improving performance under equilibrium.
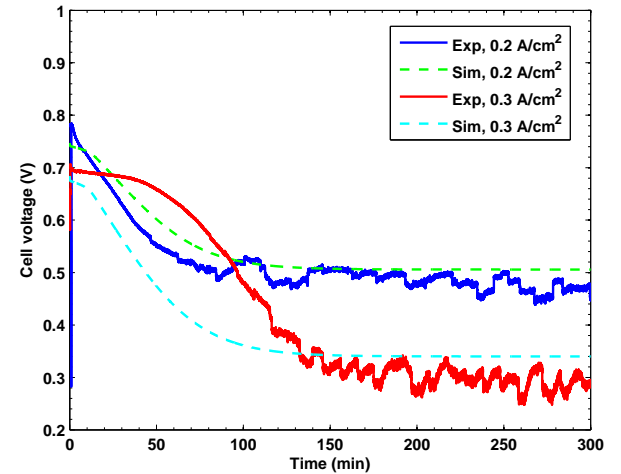

Fig. 4. The model predicted and experimental voltage evolution towards equilibrium in DEA operation. The operating conditions are 65°C cell temperature, 60% cathode supply RH, 4.0/2.4 psig anode/cathode pressure, and 2.5 cathode SR. The equilibria have been reached with current density of 0.2 and 0.3 A/cm^2

III. EVOLUTION TOWARDS EQUILIBRIUM

The model predicted spatiotemporal species evolution towards equilibrium is shown in Fig. 5 in addition to the voltage evolution. The molar fractions of nitrogen and hydrogen at times are plotted. Indeed, an equilibrium of nitrogen distribution in the channel has been established after ~100 minutes of DEA operation, with hydrogen starvation observed at the channel end. After 2500 s, only slight changes of molar fraction have been observed. The hydrogen starvation, or nitrogen blanketing, stops the local reaction and therefore the convective transport of gas mixture. The nitrogen blanketing front develops towards the channel inlet and stops at equilibrium. Thus, it is possible to derive a reduced order equation pertaining to the nitrogen blanketing front, which determines the existence of equilibrium. Such reduced order system would enable the stability analysis as compared to the full order system in Table I, and guide the design of flow channel.

Motivated by this expectation, we perform the following analysis focusing on a criteria for achieving an equilibrium based on the N$_2$ blanketing front in the anode. As shown in Table I, the governing equation for N$_2$ in anode channel (P$_{N_2}^{AN}$) from the inlet to the nitrogen blanketing front L* (y^{N_2} in Fig. 1) is:

$$\frac{1}{RT}\frac{\partial P_{N_2}^{AN}}{\partial t} = \frac{\partial}{\partial y}\left(\frac{D_{N_2}}{RT}\frac{\partial P_{N_2}^{AN}}{\partial y} - \frac{P_{N_2}^{AN}v}{RT}\right)$$
$$-K_{N_2}\frac{P_{N_2}^{CA} - P_{N_2}^{AN}}{\delta_{mb}h_{an}} \qquad (1)$$

in which P$_{N_2}^{CA}$ is the N$_2$ partial pressure in the cathode in Pa, D$_{N_2}$ is the Fickian diffusivity of N$_2$ in m^2 s^{-1}, v is the gas mixture velocity in m s^{-1}, K$_{N_2}$ is the N$_2$ permeation coefficient in mol Pa^{-1} m^{-1} s^{-1}, δ_{mb} is the membrane thickness and h$_{an}$ is the anode channel height. Once the
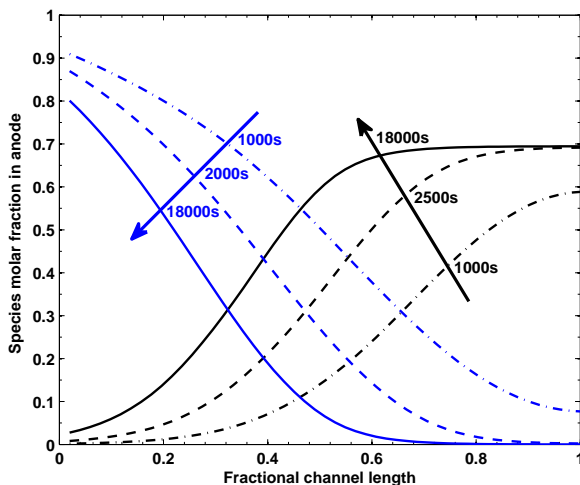
Fig. 5. The model predicted spatiotemporal N_2/H_2 molar fraction evolution towards equilibrium in DEA operation. The operating conditions are 65°C cell temperature, 60% cathode supply RH, 4.0/2.4 psig anode/cathode pressure, 2.5 cathode SR, and 0.2 A/cm^2 current density. The molar fractions at three times, 1000s, 2500s and 18000s, are shown.

operating conditions are given, δ_{mb} and h_{an} are two design variables.

From the nitrogen blanketing front L^* to the channel end, there is no hydrogen and therefore $P_{N_2}^{AN} = P^{AN} - P_{sat}$, where P^{AN} is the anode pressure and P_{sat} is the vapor saturation pressure at the given temperature. Oxygen crossover from cathode is neglected.

There are several assumptions. First, $P_{N_2}^{CA}$ is assumed to be constant along the cathode channel given the high stoichiometry ratio in the cathode, namely, the small drop of N_2 partial pressure along the channel is neglected. Second, the gas mixture velocity v is assumed to be linear along the channel in order to obtain the analytical solution of Eq. 1. At the channel inlet y=0, $v=v_i$ and at y=L^*, $v=0$; therefore $v = -\frac{v_i}{L^*}y + v_i$. Third, the membrane permeation coefficient K_{N_2} is assumed to be constant along the channel, that is, the membrane hydration and temperature are constant along the channel. Finally, D_{N_2} is assumed to be constant along the channel, which is a normal approach in fuel cell modeling [22], [23]. The effect of liquid water on diffusivity is neglected.

The validity of these assumptions is investigated by simulation of the full order system in Table I. As shown in Fig. 6, $P_{N_2}^{CA}$ indeed shows negligible variation along the channel under equilibrium. Note that the non-monotonic distribution comes from a combined effect of local oxygen/vapor partial pressure determined by local current. Since the cathode pressure is maintained constant, the decreasing oxygen partial pressure along the channel tends to produce monotonically increasing partial pressure of nitrogen, whereas the increasing vapor partial pressure leads to an opposite trend. The turning point in the subplot for $P_{N_2}^{CA}$ indicates the location where the effect of vapor pressure becomes less dominant as it approaches to saturation pressure. Gas mixture velocity v exhibits a quadratic profile along the channel and reaches zero at L^*, the linear approximation being also reasonable.

However, the permeation coefficient K_{N_2} at the channel end is two-folded of that at the inlet region, due to the low RH in the inlet and self-humidification along the channel. The simplification of constant K_{N_2} is not ideal but useful in the reduced-order system. In reality, the cathode supply RH should be increased as much as possible to approach or achieve uniform membrane hydration and therefore constant K_{N_2} along the channel.
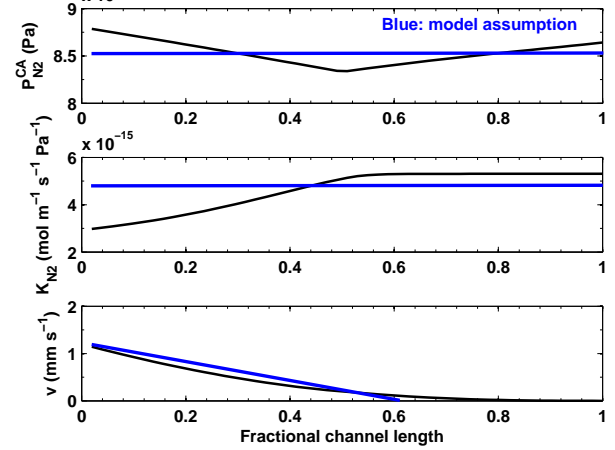

Fig. 6. The model predicted $P_{N_2}^{CA}$, K_{N_2} and v under equilibrium and their values under assumption (in blue). The operating conditions are 65°C cell temperature, 60% cathode supply RH, 4.0/2.4 psig anode/cathode pressure, 2.5 cathode SR, and 0.2 A/cm^2 current density.

With these assumptions and steady state condition, Eq. 1 can be simplified:

$$\frac{\partial^2 P_{N_2}^{AN}}{\partial y^2} + \left(\frac{v_i}{D_{N_2}L^*}y - \frac{v_i}{D_{N_2}}\right)\frac{\partial P_{N_2}^{AN}}{\partial y}$$
$$+\left(\frac{RTK_{N_2}}{D_{N_2}\delta_{mb}h_{an}} + \frac{v_i}{D_{N_2}L^*}\right)P_{N_2}^{AN} - \frac{RTK_{N_2}}{D_{N_2}\delta_{mb}h_{an}}P_{N_2}^{CA} = 0$$
(2)

The above equation can be written in a concise form where C_0 to C_3 indicate the constant coefficients:

$$\frac{\partial^2 P_{N_2}^{AN}}{\partial y^2} + (C_3 y - C_2)\frac{\partial P_{N_2}^{AN}}{\partial y} + C_1 P_{N_2}^{AN} + C_0 = 0 \quad (3)$$

in which $C_0 = -\frac{RTK_{N_2}}{D_{N_2}\delta_{mb}h_{an}}P_{N_2}^{CA}$, $C_1 = \frac{RTK_{N_2}}{D_{N_2}\delta_{mb}h_{an}} + \frac{v_i}{D_{N_2}L^*}$, $C_2 = \frac{v_i}{D_{N_2}}$, and $C_3 = \frac{v_i}{D_{N_2}L^*}$.

This is a non-linear 2nd order ODE, the exact solution consists of a homogeneous solution and a particular solution:

$$P_{N_2}^{AN} = P_h + P_p \quad (4)$$

in this case the particular solution P_p is simply $-\frac{C_0}{C_1}$. Therefore the focus is to find the solution p_h to:

$$\frac{\partial^2 P_{N_2}^{AN}}{\partial y^2} + (C_3 y - C_2)\frac{\partial P_{N_2}^{AN}}{\partial y} + C_1 P_{N_2}^{AN} = 0 \quad (5)$$

According to Ref. [24], the solution to Eq. 5 can be written

as:

$$P_h = k_1 \Phi\Big(\frac{C_1}{2C_3}, \frac{1}{2}, -\frac{C_3}{2}(y-L^*)^2\Big)$$
$$+ k_2 y^{\frac{1}{2}} \Phi\Big(\frac{C_1}{2C_3} + \frac{1}{2}, \frac{3}{2}, -\frac{C_3}{2}(y-L^*)^2\Big) \tag{6}$$

in which Φ is the Kummer's function, k_1 and k_2 are two constants to be determined by the boundary conditions, i.e., $\frac{\partial P_{N_2}^{AN}(0)}{\partial y}=0$, and $P_{N_2}^{AN}(L^*)=P^{AN}\text{-}P_{sat}$.

Having the analytical solution available, an equilibrium of N_2 distribution in the anode can be established by a mass conservation:

$$\frac{A_{ch}K_{N_2}}{\delta_{mb}h_{an}}\int_0^{L^*}[P_{N_2}^{CA} - P_{N_2}^{AN}(y)]dy - \frac{A_{ch}K_{N_2}}{\delta_{mb}h_{an}}(P^{AN}$$
$$-P_{sat}-P_{N_2}^{CA})(L_{ch}-L^*)=0 \tag{7}$$

where A_{ch} is the anode channel cross section area. Eq. 7 states that the average N_2 crossover rate in the non-blanketing region from cathode to anode equals to that in the blanketing region from anode to cathode. It can be further simplified to:

$$\int_0^{L^*} P_{N_2}^{AN}(y)dy - P_{N_2}^{CA}$$
$$+(P^{AN}-P_{sat})(L_{ch}-L^*)=f(L^*)=0 \tag{8}$$

The existence of solution to Eq. 8, an algebraic equation, determines the existence of equilibrium of N_2 blanketing front evolution in the anode. Note that the fuel cell design variables δ_{mb} and h_{an} and operating parameters other than pressure are implicitly shown in Eq. 8 since they enter the $P_{N_2}^{AN}(y)$ function from k_1 and k_2 via boundary conditions. It is possible to choose appropriate fuel cell design variables and operating conditions to obtain the solution to Eq. 8.

IV. Conclusions

In this paper, we investigated the nitrogn blanketing front equilibrium in dead-ended anode operation when the purge is disabled. The equilibrium mechanism can be summarized as zero net flux of nitrogen crossover through the membrane. For a wide range of cathode pressure and RH, the simulation results using tuned model match the experimental data with satisfactory accuracy. Both simulation using tuned model and experimental data indicate the voltage evolution towards equilibrium under certain operating conditions.

We simplified the full-order-model to a second order non-homogeneous ODE with one state by assuming constant cathode partial pressure and membrane permeation coefficient of nitrogen along the channel, as well as a linear profile of gas mixture velocity in the anode. The ODE was solved to obtain an algebraic constraint for nitrogen blanketing front L^*. The existence of solution to this algebraic constraint becomes a criteria for determining the existence of nitrogen blanketing equilibrium. The order reduction approach shown in this paper aids the equilibrium analysis and guide the channel/membrane design of a DEA cell, although the effect of such approach needs further investigation when an explicit form of solution is found and a comparison with the numerical simulation of the full-order-model is performed.

References

[1] P. Mocoteguy, F. Druart, Y. Bultel, S. Besse, and A. Rakotondrainibe, "Monodimensional modeling and experimental study of the dynamic behavior of proton exchange membrane fuel cell stack operating in dead-end mode," *Journal of Power Sources*, vol. 167, pp. 349–357, 2007.

[2] D. McKay, J. Siegel, W. Ott, and A. Stefanopoulou, "Parameterization and prediction of temporal fuel cell voltage behavior during flooding and drying conditions," *Journal of Power Sources*, vol. 178, pp. 207–222, 2008.

[3] J. Siegel, D. McKay, A. Stefanopoulou, D. Hussey, and D. Jacobson, "Measurement of liquid water accumulation in a PEMFC with dead-ended anode," *Journal of Electrochemical Society*, vol. 155, pp. B1168–B1178, 2008.

[4] C. A. Ramos-Paja, C. Bordons, A. Romero, R. Giral, and L. Martnez-Salamero, "Minimum fuel consumption strategy for PEM fuel cells," *IEEE Transactions on Industrial Electronics*, vol. 56, pp. 685–696, 2009.

[5] T. Matsuura, J. Siegel, J. Chen, and A. Stefanopoulou, "Multiple degradation phenomena in polymer electrolyte fuel cell operation with dead-ended anode," *Proceeding of ASME 2011 5th International Conference on Energy Sustainability & 9th Fuel Cell Science, Engineering and Technology Conference*, Washington D.C., 2011.

[6] P. Rodatz, G. Paganelli, and L. Guzzella, "Optimizing air supply control of a PEM fuel cell system," in *Proceedings of American Control Conference*, vol. 3, 2003, pp. 2043–2048.

[7] K. Promislow, J. St-Pierre, and B. Wetton, "A simple, analytic model of polymer electrolyte membrane fuel cell anode recirculation at operating power including nitrogen crossover," *Journal of Power Sources*, vol. 196, pp. 10 050–10 056, 2011.

[8] S. Hikita, F. Nakatani, K. Yamane, and Y. Takagi, "Power-generation characteristics of hydrogen fuel cell with dead-end system," *JSAE Review*, vol. 23, pp. 177–182, 2002.

[9] J. Chen, J. B. Siegel, and A. G. Stefanopoulou, "Nitrogen blanketing front equilibria in dead end anode fuel cell operation," in *American Control Conference*, San Francisco, CA, 2011.

[10] A. Manokaran, S. Pushpavanam, P. Sridhar, and S. Pitchumani, "Experimental analysis of spatio-temporal behavior of anodic dead-end mode operated polymer electrolyte fuel cell," *Journal of Power Sources*, vol. 196, pp. 9931–9938, 2011.

[11] E. Muller, F. Kolb, L. Guzzella, A. Stefanopoulou, and D. McKay, "Correlating nitrogen accumulation with temporal fuel cell performance," *Journal of Fuel Cell Science and Technology*, vol. 7, pp. 021 013–1–021 013–11, 2010.

[12] J. Siegel, S. Bohac, A. Stefanopoulou, and S. Yesilyurt, "Nitrogen front evolution in purged polymer electrolyte membrane fuel cell with dead-ended anode," *Journal of Electrochemical Society*, vol. 157, pp. B1081–B1093, 2010.

[13] J. Chen, J. B. Siegel, T. Matsuura, and A. G. Stefanopoulou, "Carbon corrosion in PEM fuel cell dead-ended anode operations," *Journal of Electrochemical Society*, vol. 158, pp. B1164–B1174, 2011.

[14] J. Chen, J. B. Siegel, and A. G. Stefanopoulou, "Optimization of purging cycle for dead-ended anode fuel cell operation," *International Journal of Hydrogen Energy*, vol. submitted, 2012.

[15] J. F. Moxley, S. Tulyani, and J. B. Benziger, "Steady-state multiplicity in the autohumidification polymer electrolyte membrane fuel cell," *Chemical Engineering Science*, vol. 58, pp. 4705–4708, 2003.

[16] J. Benziger, E. Chia, E. Karnas, J. Moxley, C. Teuscher, and I. Kevrekidis, "The stirred tank reactor polymer electrolyte membrane fuel cell," *AIChE Journal*, vol. 50, pp. 1889–1990, 2004.

[17] W. Hogarth and J. Benziger, "Operation of polymer electrolyte membrane fuel cells with dry feeds: Design and operating strategies," *Journal of Power Sources*, vol. 159, pp. 968–978, 2006.

[18] C. Woo and J. Benziger, "PEM fuel cell current regulation by fuel feed control," *Chemical Engineering Science*, vol. 62, pp. 957–968, 2007.

[19] J. Siegel, A. Stefanopoulou, G. Ripaccioli, and S. Di Cairano, "Purge Scheduling for Dead-Ended Anode Operation of PEM Fuel Cells" *The Control Handbook: Control System Applications, Second Edition*, W. S. Levine, Ed. CRC Press, 2010.

[20] D. Curtin, R. Lousenberg, T. Henry, P. Tangeman, and M. Tisack, "Advanced materials for improved PEMFC performance and life," *Journal of Power Sources*, vol. 131, pp. 41–48, 2004.

[21] A. Weber, "Gas-crossover and membrane-pinhole effects in polymer-electrolyte fuel cells," *J. Electrochem. Soc.*, vol. 155, pp. B521–B531, 2008.

[22] Y. Wang and C.-Y. Wang, "Modeling polymer electrolyte fuel cells with large density and velocity changes," *Journal of Electrochemical Society*, vol. 152, pp. A445–A453, 2005.

[23] K. Jiao and X. Li, "Three-dimensional multiphase modeling of cold start processes in polymer electrolyte membrane fuel cells," *Electrochimica Acta*, vol. 54, pp. 6876–6891, 2009.

[24] A. D. Polyanin and V. F. Zaitsev, *Handbook of Exact Solutions for Ordinary Differential Equations*. Chapman & Hall/CRC, 2003.